Low-nonlinearity spin-torque oscillations driven by ferromagnetic nanocontacts

Muftah Al-Mahdawi,* Yusuke Toda, Yohei Shiokawa, and Masashi Sahashi
Department of Electronic Engineering, Tohoku University, Sendai 980-8579, Japan
(Received 29 March 2015; revised manuscript received 26 December 2015; published 14 January 2016)

Spin-torque oscillators are strong candidates as nanoscale microwave generators and detectors. However, because of large amplitude-phase coupling (nonlinearity), phase noise is enhanced over other linear autooscillators. One way to reduce nonlinearity is to use ferromagnetic layers as a resonator and excite them at localized spots, making a resonator-excitor pair. We investigated the excitation of oscillations in dipole-coupled ferromagnetic layers, driven by localized current at ferromagnetic nanocontacts. Oscillations possessed properties of optical-mode spin waves and at low field (≈200 Oe) had high frequency (15 GHz), a moderate precession amplitude (2°–3°), and a narrow spectral linewidth (<3 MHz) due to localized excitation at nanocontacts. Micromagnetic simulation showed emission of the resonator's characteristic optical-mode spin waves from disturbances generated by domain-wall oscillations at nanocontacts.

DOI: 10.1103/PhysRevB.93.024408

I. INTRODUCTION

Transfer of angular momentum from a dc spin-polarized current to a nanoscale ferromagnet (FM) exerts an antidamping torque, spin-transfer torque (STT), that can compensate intrinsic damping torque and induce stable precession of magnetization [1]. When combined with a magnetoresistance effect, like giant magnetoresistance (GMR) or tunneling magnetoresistance (TMR), high-frequency voltage oscillations are emitted, producing spin-torque oscillations (STO) [2]. The same structures can also rectify injected ac voltage at resonance [3,4], and off-resonance [5]. Such microwave nanooscillators/detectors are sought after for applications like inter-/intrachip communication, imaging [6], nondestructive testing, and laboratory-on-chip sensors. STOs are suitable candidates for such a role. However, low output power, the trade-off between power and frequency, and weak coherence of oscillations hinder their applications compared with their semiconductor counterparts. The large nonlinear phase-amplitude coupling [7] produces a dilemma between large precession amplitude and small linewidth. Also, frequency locking of STOs to the external reference signal becomes hindered [8]. Such a dilemma can be overcome by the separation of STOs into an excitation source and a resonating element, so that precession frequency and amplitude will be set by the resonator design, not by the driving STT. Then the linewidth will be reduced considerably.

It was shown that nonuniform current density in TMR-STO resulted in an increase in the amplitude of generated precession [9,10], and a reduction in linewidth [9,11–13]. However, the origin is still not clear, and the fabrication process is not well understood or easily reproducible. On the other hand, the ion-assisted oxidation (IAO) of ultrathin aluminum reproducibly was used to fabricate a 1-nm-thin alumina nanooxide layer (NOL) with direct 2-nm nanocontacts (NCs) between FM layers [14–18]. In NOL-based STOs, moderate power and narrow linewidths were reported [19–22], with oscillation behavior similar to low-TMR-STO [23]. There is evidence for the presence of FM metallic NCs by magnetoresistance and transport properties [15], transmission-electron micrographs [16,18,24], and conductive atomic force microscopy [16,17,24]. However, the measured nanocontacts magnetoresistance (NCMR) ratios are far below expectation compared with scattering from confined domain walls (DW) [25–27], mostly due to the presence of oxygen and nonmagnetic impurities [17,24,28].

In this paper, we propose that the localized precession of DWs at NCs work as excitors of spin waves in FM layers. This makes frequency completely determined by the resonator's designed eigenfrequency, regardless of the mechanism of excitors. The loss of frequency tunability reduces nonlinearity and linewidth considerably. After the experimental and simulation description, we present the excited modes in the chosen resonator, then we discuss the reduced nonlinearity of NCMR-STO. For the resonator, we used a nanopillar with two free FM layers, where the magnetostatic dipolar field provides interlayer coupling with two coupled-oscillation characteristic modes [29]. The dynamics of coupled free FM layers are of practical interest for high-frequency emission at low applied field (<500 Oe), linewidth narrowing, and doubling of magnetization precession frequency in resistance oscillations [30–33]. Most importantly, the loss of current tunability of frequency can be compensated by the controllability of interlayer relative angle.

II. EXPERIMENT AND SIMULATION

The film stack with designed thickness in nanometers was as follows: thermally oxidized silicon substrate/electrode layer (Ta 5/Cu 200/Ta 40/chemical-mechanical polishing)/milling 5/Ta 3/Ru 2/$Fe_{50}Co_{50}$ 5/Al 1.3/IAO 20 seconds exposure time/Al 0.3/$Fe_{50}Co_{50}$ 5/capping (Cu 10/Ru 10). The film was deposited by magnetron and ion-beam sputtering in the chambers described before [17]. Subsequently, films were vacuum annealed at 270°C and 400°C for 1.5 h each with 10-kOe magnetic field. The additional metal Al insertion and the choice of capping material were optimized with the annealing process for lower resistance-area (RA) product and enhanced MR ratio, based on previous work [17,28]. Current-perpendicular-to-plane (CPP) pillars of the elliptical cross section were microfabricated by Ar^+ ion milling and

*mahdawi@ecei.tohoku.ac.jp

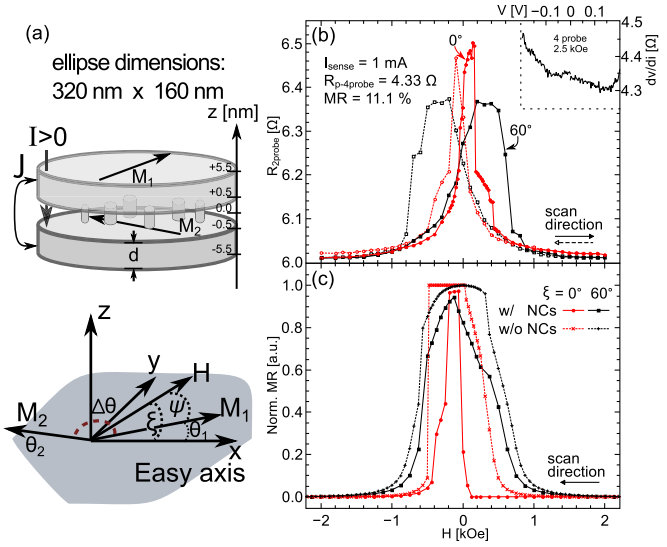

FIG. 1. (a) A schematic of the elliptical pillar geometry and definitions of coordinates and angles. (b) Two-probe resistance vs field applied at $\xi = 0^\circ$ and 60°. Inset shows the bias dependence of differential resistance in parallel magnetizations state. (c) Normalized MR found from micromagnetics simulation, for the cases of no NCs (dashed lines), and with 20 NCs (solid lines).

electron-beam lithography. RA was found from the slope of four-probe dc resistance vs the area inverse (R-1/A) line, and compared with current-in-plane-tunneling (CIPT) measurement of unpatterned films.

The STO microwave emissions were measured by a 26-GHz spectrum analyzer under biasing from a bias T, and scattering at the measurement probe was measured by a network analyzer. Geometry, angles, and coordinate definitions are summarized in Fig. 1(a). The positive current was defined to be electrons flowing up. We are presenting the detailed measurements of a 320 nm $\times$ 160 nm pillar at $\xi = 60^\circ$, although results presented later were qualitatively similar among samples.

Micromagnetic simulation was done by NMAG, a finite-element-method simulator [34]. Calculation geometry consisted of two ellipses the same as experimental design separated by 1 nm, and NCs were included as 1-nm-radius cylindrical contacts between the two layers. The interlayer dipolar field was included through the demagnetization field calculation. Material parameters are as follows: stiffness constant of 2.3×10^{-10} erg/cm^3, saturation magnetization of 1930 emu/cm^3 [35], with Gilbert damping constant of 0.02, and an unphysical spin polarization of 100%. Mesh size away from NCs was set to 5 nm, and it changed to 0.7 nm inside NCs. For hysteresis loops, ξ dependence was calculated for 20 randomly placed NCs. For qualitative understanding of STO dynamics, we compared the cases of zero and four NCs, under the experimental conditions of the 250-Oe field applied at $\xi = 60^\circ$. The current profile was approximated to be confined in NCs with confinement extending 1 nm away from the middle of NC into FM layers, as most of the voltage drop will be on this region [36], although more accurate representation is needed [37]. The total current was +17.5 mA and the current distribution was calculated by assuming that a single NC and tunnel barrier resistances are 600 Ω and 500 Ω, respectively [16].

III. RESULTS AND DISCUSSION

RA found from the slope of the four-probe R-1/A line, and CIPT measurements were 0.2 and 0.3 Ω μm^2, respectively. The bias dependence of four-probe differential resistance at the parallel magnetization state [inset in Fig. 1(b)] was relatively flat. The resistance temperature dependence of similarly conditioned films also showed metallic-transport character. This indicates that conduction is dominated by transport through NCs and not by tunneling through the oxide barrier. Previously, high-temperature annealing (>380°C) was hindered by manganese diffusion from pinning the antiferromagnet towards NOL [17]. Better NOL barrier quality and purer NCs were obtained in this report by using a manganese-free structure for higher annealing temperature, in addition to insertion and capping layer optimizations [28].

Figure 1(b) shows the two-probe resistance vs magnetic field (R-H) applied at $\xi = 0^\circ$ and 60° measured at the same position as STO measurements. From the switching fields of easy-axis R-H, interlayer dipolar coupling field (H_{ic}) is estimated at 400 Oe. It is in agreement with the estimation of cross-demagnetization [38], $H_{ic} = 4\pi\rho_{12}M_s = 433$ Oe, where $M_s = 1750$ emu/cm^3 is the measured saturation magnetization, and $\rho_{12} = 0.0197$ is the cross-demagnetization factor. This dipole interlayer coupling can be considered equivalent to the usual bilinear coupling through a metal spacer ($J = -2dM_sH_{ic} = -0.7$ erg/cm^2 [39], defined negative for antiparallel coupling). The contribution from coupling through NCs and spacer roughness to magnetostatic energy can be neglected. Ferromagnetic coupling was found to be small from the free-layer magnetization-loop shift of unpatterned spin-valve films (IrMn/FeCo(pinned)/NOL-NCs/FeCo(free)), with $J_{NCs} = 0.01$–0.02 erg/cm^2 [17].

Micromagnetic simulation reproduced static R-H, H_{ic} estimation, and the reduction of AP-to-P plateau width by NCs [Fig. 1(c)]. We chose for oscillation measurements the pillar that had the closest R-H curve to the micromagnetic simulation, which had 11.1% MR ratio and 0.17 Ω μm^2 RA product. Due to large pillar size, uniform rotational switching was not reproducible for the field applied along the easy axis ($\xi = 0^\circ$). At tilted angles, the magnetization rotated as a single domain. Thus we are presenting tilted angle results of oscillations (Fig. 2).

Largest power microwave oscillations were observed for $\xi = 60^\circ$ at ≈15 GHz when applying high currents. Sample power spectrum with a Lorentzian peak fitting is shown in Fig. 2(a). There is a drop in resistance at $I_{dc} = 14.7$ mA accompanied with a jump in oscillation frequency f_{osc}, a narrowing in full width at half maximum Δf, and an increase in integrated power P_{int}, indicating a change into autooscillation mode [40], with a mechanism similar to STOs based on pin-hole tunnel junctions [Fig. 2(c)] [9]. Linear fits to normalized inverse power $1/p$ at subthreshold gave a threshold current I_{th} of 14.74 mA. The presence of two frequency branches at subthreshold and high-current regions can be ascribed to edge and center modes in elliptical geometries [41]. The highest oscillation power is 0.4 nW (1.6 nW if corrected

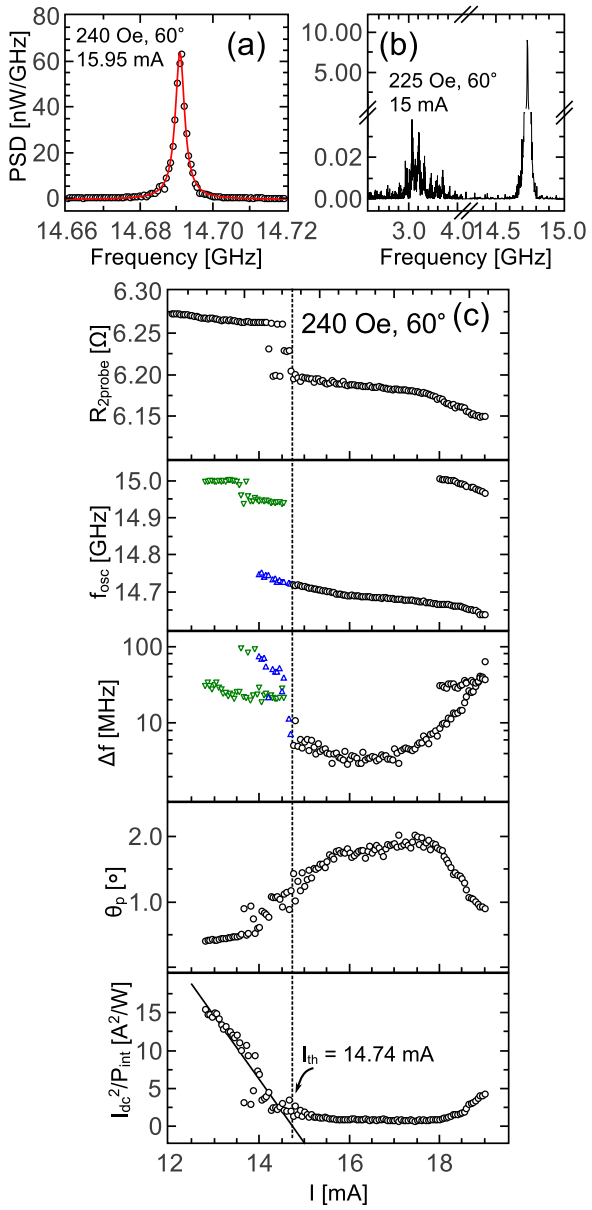

FIG. 2. (a) Representative oscillation power spectrum at $\xi = 60^\circ$ with Lorentzian peak fitting (solid line). (b) The acoustic and optical modes of coupled oscillations were observed near 3 GHz and 15 GHz, respectively. (c) Current dependencies of oscillation characteristics. Same symbols in $f_{\rm osc}$ and Δf panels correspond to each other.

for impedance mismatch) giving a precession amplitude (θ_p) of 2°–3°, whereas the lowest Δf is 3 MHz corresponding to a quality factor of 5000.

Regarding the excited oscillations, the possible coupled oscillations or spin waves in two layers of free spins are the optical (antiphase) mode (OM) and the acoustic (in-phase) mode (AM) [29]. Mode frequencies can be found from the solution to coupled Bloch equations of the two layers with the effective field determined from the free energy [39,42,43]. We considered only the main contributions of Zeeman energy, film demagnetization, and interlayer dipolar coupling. The optical and acoustic eigenfrequencies of an in-plane magnetization precession can be simplified to

$$\left(\frac{f_{\rm ac}}{\gamma/2\pi}\right)^2 = (H\cos\psi + 4\pi M_s - 2H_{\rm ic}(\cos\Delta\theta + 1)) \times (H\cos\psi) + 8H_{\rm ic}^2\cos\Delta\theta, \quad (1a)$$

$$\left(\frac{f_{\rm op}}{\gamma/2\pi}\right)^2 = (H\cos\psi + 4\pi M_s - 2H_{\rm ic}(\cos\Delta\theta + 1)) \times (H\cos\psi - 4H_{\rm ic}\cos\Delta\theta), \quad (1b)$$

where $\gamma/2\pi = 2.8$ MHz/Oe is the gyromagnetic ratio, and other symbols are defined in Fig. 1(a). We confirmed the presence of the weaker-amplitude AM [Fig. 2(b)]. Using $H_{\rm ic} = 400$ Oe and $\Delta\theta = 130^\circ$–150° from measured R-H and micromagnetic simulation results in $f_{\rm op}$ of 14.0–16.1 GHz and $f_{\rm ac}$ of 3.9–3.5 GHz, which agrees with the observed spectrum. The frequency of OM depends mostly on the coupling strength and relative angle between the layers [the last term on the right in Eq. (1b)]. The weak dependence of $f_{\rm osc}$ against $I_{\rm dc}$ and H (≈ -1.3 MHz/Oe not shown) supports that $f_{\rm osc}$ is determined mainly by excitation of an OM spin wave. The maximum $f_{\rm osc}(H = 0, \Delta\theta = 180^\circ)$ from other devices was 17.8 GHz which corresponds to $H_{\rm ic} = 460$ Oe, in agreement with the estimation from the corresponding R-H curve. To increase the oscillation frequency, we reduced the size of the elliptical pillars to 160 nm × 80 nm. At $I_{\rm dc} = 2.8$ mA, $H = 185$ Oe, and $\xi = 50^\circ$, the resulting oscillations had $f_{\rm osc}$, $df/dI_{\rm dc}$, and Δf of 23.3 GHz, <4 MHz/mA, and 1.3-MHz linewidth, respectively. The corresponding quality factor is more than 17 000.

Although the presented frequency of OM is higher than AM, the measured and simulated peak intensities of OM are much larger [Figs. 2(b) and 3(a) and 3(c)]. This is due to two reasons. In OM, antiphase dynamics maximize dynamic MR change [31,32]. In comparison, OM amplitude as measured by Brillouin light scattering is reduced due to canceling contributions to the light scattering cross section [39]. Secondly, the energy required to excite OM is smaller in anticoupled ($J < 0$) harmonic oscillators. The average energy difference between AM and OM with equal precession amplitudes is $\langle E_{\rm ac}\rangle - \langle E_{\rm op}\rangle = -J(\delta\mathbf{m}_1 \cdot \delta\mathbf{m}_2)$, where $\delta\mathbf{m}_1 \cdot \delta\mathbf{m}_2$ is the characteristic mode's dimensionless power. For $J < 0$, excitation of AM requires higher energy than same-amplitude OM.

It should be noted that Eqs. (1) were derived for infinite-wavelength limit (i.e., wave-vector-thickness product $qd \approx 0$). Quantitative corrections due to dynamic dipolar coupling between propagating spin waves cannot be ignored because $qd = 1.74$ from simulation presented later [39,42,43]. But due to experimental uncertainty in determining $H_{\rm ic}\cos\Delta\theta$, an exact quantitative comparison becomes difficult, and the main conclusions are not changed.

The linewidth broadening of STOs compared to linear autooscillators is understood to be due to amplitude-phase coupling [7], which is expressed by the nonlinearity parameter (ν) [44]. The nonlinearity of presented results is $\nu = (I_{\rm dc}/\Gamma_g)(df/dI_{\rm dc}) \approx -0.16$. The natural FMR linewidth ($\Gamma_g = 934$ MHz) is obtained from linear extrapolation of Δf to zero current at subthreshold [45], and the agility of oscillation frequency in current ($df/dI_{\rm dc}$) was −9.6 MHz/mA.

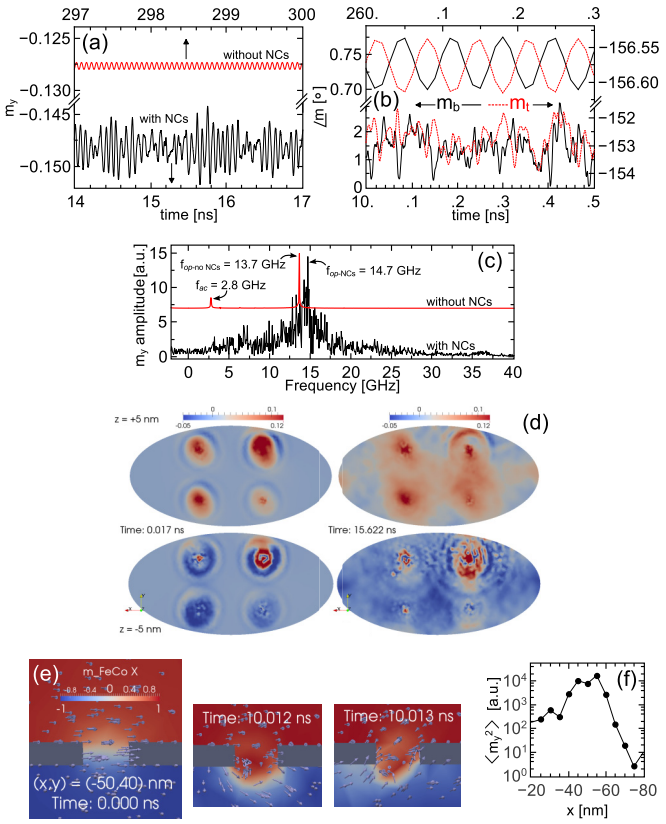

FIG. 3. (a)–(c) Comparison of micromagnetic dynamics with (top part) or without (bottom part) NCs at $H = 250$ Oe, $\xi = 60^\circ$, $I_{dc} = 17.5$ mA. (a) Normalized magnetization's y component of the total system (m_y). (b) Magnetization angle of top and bottom layers at $(x,y) = (0,0)$. (c) Spectrum of m_y transformed from 250-ns (15-ns) duration of dynamics without (with) NCs. (d) Time snapshots with the color representing $[m_y(\mathbf{r},t) - m_y(\mathbf{r},0)]$. Optical-mode spin waves are emitted from localized excitation at NCs. (e) The origin of localized excitation is a confined domain wall that is oscillating at 250 GHz. (f) Power profile of localized precession around the top-right NC.

This nonlinearity is one order of magnitude smaller than other reported values [13,45,46]. Because the nonlinearity is very small, the sudden change of oscillation into a single mode at threshold hinders the applicability of determining ν from the Δf-$1/p$ plot [13]. The Δf-$1/p$ slopes were 3.8 and 19.4 MHz/(mA^2 μW) for above-threshold and below-threshold regimes, respectively.

NCMR-STO usually showed relatively small agility (16–18 MHz/mA) [19,21,23] compared with other TMR-STOs, leading to smaller nonlinearity and narrow linewidth. Possible reasons for lowered agility and nonlinearity in this report can be the optimized fabrication process with purer NCs [17,28], the coupled oscillations of two layers [31,33,47], and the tilted magnetization angle away from the easy axis [48]. However, the loss of agility and small linewidths were obtained for various angles and frequencies, which indicates that the improved purity of NCs is the main factor.

We used micromagnetic simulation to show how nanomagnets with NCs worked as a resonator-excitor pair. Results shown in Fig. 3 agree reasonably with experimental data. In the case of no NCs [upper part in Figs. 3(a)–3(c)] oscillation frequency is similar to the calculated and measured ones, with the optical mode being the dominant component. But precession amplitude ($\theta_p = 0.05^\circ$) is very small compared with the experimental value (2°–3°). With the insertion of four NCs, optical spin waves were emitted from NCs [Fig. 3(d)], and increased θ_p to 2° [lower part in Figs. 3(a)–3(c)]. The origin of perturbation near NCs is of similar origin to previous reports [49,50]. The domain wall is pushed outside the NC region into the ferromagnetic layer and starts to oscillate at high frequency between Néel and Bloch walls (250 GHz for the chosen geometry and current density) [Fig. 3(e)]. These very high frequency oscillations were localized up to 5–10 nm away from NC [Fig. 3(f)]. The localized precession acts as a point source that generates spin waves propagating radially at the characteristic mode of the system, which is an optical spin wave.

The implication on the nature of current-induced dynamics is that magnetization precession is not induced by STT directly. In Fig. 2(c), at first going above I_{th}, localized STT increases amplitude, compensates damping around NCs and increases local precession amplitude. When local precession amplitude saturates, at $I = 15.6$ mA, increase of current and STT will not change θ_p, leading to loss of agility and narrowing of linewidth. At this stable regime, magnetic layers act as a resonator that is excited by the energy coming from the point sources at NCs. This makes the presented oscillator similar to a classical autooscillator, and results in a considerable reduction in linewidth.

IV. CONCLUSION

In conclusion, we presented the measured spin-torque-driven oscillations of a spin-torque oscillator with nanocontacts between two free ferromagnetic layers coupled antiferrmagnetically with the dipolar field. Resulting oscillation character agrees with propagating optical-mode spin waves. In micromagnetic simulation, inclusion of NCs with localized current density showed that NCs work as point sources, and optical-mode spin waves were excited in the ferromagnetic layers. The ferromagnetic layers act as a resonator that is decoupled from mechanism of excitation point sources. Since oscillation is not driven by the spin-transfer torque, linewidth decreased.

Although we studied dual ferromagnetic layers in this report, the same effect should be the origin for the small nonlinearity and linewidth narrowing common in NCMR and pin-hole-TMR STOs [9,11,19,21,23]. So, by utilizing NCs and using a magnetic resonator that has a large oscillation amplitude, e.g., tilted-anisotropy ferromagnets [51], we expect to increase both power and quality factor for applications.

ACKNOWLEDGMENTS

The authors would like to thank Dr. Andrei Slavin for his insightful comments and discussion. This work was supported by the SCOPE program (Contract No. 0159-0058) from Ministry of Internal Affairs and Communications.

[1] J. C. Slonczewski, U.S. Patent No. 5,695,864 (1997).

[2] S. I. Kiselev, J. C. Sankey, I. N. Krivorotov, N. C. Emley, R. J. Schoelkopf, R. A. Buhrman, and D. C. Ralph, Nature (London) **425**, 380 (2003).

[3] A. A. Tulapurkar, Y. Suzuki, A. Fukushima, H. Kubota, H. Maehara, K. Tsunekawa, D. D. Djayaprawira, N. Watanabe, and S. Yuasa, Nature (London) **438**, 339 (2005).

[4] S. Miwa, S. Ishibashi, H. Tomita, T. Nozaki, E. Tamura, K. Ando, N. Mizuochi, T. Saruya, H. Kubota, K. Yakushiji, T. Taniguchi, H. Imamura, A. Fukushima, S. Yuasa, and Y. Suzuki, Nat. Mater. **13**, 50 (2014).

[5] L. Fu, Z. X. Cao, S. Hemour, K. Wu, D. Houssameddine, W. Lu, S. Pistorius, Y. S. Gui, and C. Hu, Appl. Phys. Lett. **101**, 232406 (2012).

[6] L. Fu, W. Lu, D. R. Herrera, D. F. Tapia, Y. S. Gui, S. Pistorius, and C. Hu, Appl. Phys. Lett. **105**, 122406 (2014).

[7] J.-V. Kim, V. Tiberkevich, and A. N. Slavin, Phys. Rev. Lett. **100**, 017207 (2008).

[8] B. Georges, J. Grollier, M. Darques, V. Cros, C. Deranlot, B. Marcilhac, G. Faini, and A. Fert, Phys. Rev. Lett. **101**, 017201 (2008).

[9] D. Houssameddine, S. H. Florez, J. A. Katine, J. Michel, U. Ebels, D. Mauri, O. Ozatay, B. Delaet, B. Viala, L. Folks, B. D. Terris, and M. Cyrille, Appl. Phys. Lett. **93**, 022505 (2008).

[10] H. Maehara, U.S. Patent No. 8,836,438 (2014).

[11] D. Houssameddine, U. Ebels, B. Dieny, K. Garello, J.-P. Michel, B. Delaet, B. Viala, M.-C. Cyrille, J. A. Katine, and D. Mauri, Phys. Rev. Lett. **102**, 257202 (2009).

[12] T. Devolder, L. Bianchini, J. Kim, P. Crozat, C. Chappert, S. Cornelissen, M. O. d. Beeck, and L. Lagae, J. Appl. Phys. **106**, 103921 (2009).

[13] K. Kudo, T. Nagasawa, R. Sato, and K. Mizushima, J. Appl. Phys. **105**, 07D105 (2009).

[14] H. Fukuzawa, H. Yuasa, S. Hashimoto, K. Koi, H. Iwasaki, M. Takagishi, Y. Tanaka, and M. Sahashi, IEEE Trans. Magn. **40**, 2236 (2004).

[15] H. N. Fuke, S. Hashimoto, M. Takagishi, H. Iwasaki, S. Kawasaki, K. Miyake, and M. Sahashi, IEEE Trans. Magn. **43**, 2848 (2007).

[16] M. Takagishi, H. N. Fuke, S. Hashimoto, H. Iwasaki, S. Kawasaki, R. Shiozaki, and M. Sahashi, J. Appl. Phys. **105**, 07B725 (2009).

[17] Y. Shiokawa, M. Shiota, Y. Watanabe, T. Otsuka, M. Doi, and M. Sahashi, IEEE Trans. Magn. **47**, 3470 (2011).

[18] H. Yuasa, M. Hara, Y. Fuji, and H. Fukuzawa, EPL (Europhysics Letters) **101**, 47005 (2013).

[19] H. Endo, T. Tanaka, M. Doi, S. Hashimoto, H. N. Fuke, H. Iwasaki, and M. Sahashi, IEEE Trans. Magn. **45**, 3418 (2009).

[20] H. Suzuki, H. Endo, T. Nakamura, T. Tanaka, M. Doi, S. Hashimoto, H. N. Fuke, M. Takagishi, H. Iwasaki, and M. Sahashi, J. Appl. Phys. **105**, 07D124 (2009).

[21] H. Suzuki, T. Nakamura, H. Endo, M. Doi, H. Tsukahara, H. Imamura, H. N. Fuke, S. Hashimoto, H. Iwasaki, and M. Sahashi, Appl. Phys. Lett. **99**, 092507 (2011).

[22] M. Doi, H. Endo, K. Shirafuji, S. Kawasaki, M. Sahashi, H. N. Fuke, H. Iwasaki, and H. Imamura, J. Phys. D: Appl. Phys. **44**, 092001 (2011).

[23] M. Al-Mahdawi, M. Doi, S. Hashimoto, H. N. Fuke, H. Iwasaki, and M. Sahashi, IEEE Trans. Magn. **47**, 3380 (2011).

[24] M. Al-Mahdawi and M. Sahashi, Appl. Phys. Lett. **104**, 032405 (2014).

[25] L. R. Tagirov, B. P. Vodopyanov, and K. B. Efetov, Phys. Rev. B **63**, 104428 (2001).

[26] J. Sato, K. Matsushita, and H. Imamura, J. Appl. Phys. **105**, 07D101 (2009).

[27] H. Imamura and J. Sato, J. Phys.: Conf. Ser. **266**, 012090 (2011).

[28] Y. Shiokawa, J. Jung, T. Otsuka, and M. Sahashi, J. Appl. Phys. **118**, 053909 (2015).

[29] P. Grünberg, J. Appl. Phys. **51**, 4338 (1980).

[30] T. Seki, H. Tomita, T. Shinjo, and Y. Suzuki, Appl. Phys. Lett. **97**, 162508 (2010).

[31] T. Moriyama, G. Finocchio, M. Carpentieri, B. Azzerboni, D. C. Ralph, and R. A. Buhrman, Phys. Rev. B **86**, 060411 (2012).

[32] P. M. Braganca, K. Pi, R. Zakai, J. R. Childress, and B. A. Gurney, Appl. Phys. Lett. **103**, 232407 (2013).

[33] T. Nagasawa, K. Kudo, H. Suto, K. Mizushima, and R. Sato, Appl. Phys. Lett. **105**, 182406 (2014).

[34] T. Fischbacher, M. Franchin, G. Bordignon, and H. Fangohr, IEEE Trans. Magn. **43**, 2896 (2007).

[35] K. Miyake, Y. Okutomi, H. Tsukahara, H. Imamura, and M. Sahashi, Appl. Phys. Express **6**, 113001 (2013).

[36] Y. G. Naidyuk and I. K. Yanson, *Point-Contact Spectroscopy* (Springer, New York, 2005).

[37] N. Strelkov, A. Vedyayev, N. Ryzhanova, D. Gusakova, L. D. Buda-Prejbeanu, M. Chshiev, S. Amara, N. de Mestier, C. Baraduc, and B. Dieny, Phys. Rev. B **84**, 024416 (2011).

[38] O. Dmytriiev, T. Meitzler, E. Bankowski, A. Slavin, and V. Tiberkevich, J. Phys.: Condens. Matter **22**, 136001 (2010).

[39] M. Grimsditch, S. Kumar, and E. E. Fullerton, Phys. Rev. B **54**, 3385 (1996).

[40] A. Slavin and V. Tiberkevich, IEEE Trans. Magn. **45**, 1875 (2009).

[41] A. M. Deac, A. Fukushima, H. Kubota, H. Maehara, Y. Suzuki, S. Yuasa, Y. Nagamine, K. Tsunekawa, D. D. Djayaprawira, and N. Watanabe, Nat. Phys. **4**, 803 (2008).

[42] J. F. Cochran, J. Rudd, W. B. Muir, B. Heinrich, and Z. Celinski, Phys. Rev. B **42**, 508 (1990).

[43] R. Zivieri, L. Giovannini, and F. Nizzoli, Phys. Rev. B **62**, 14950 (2000).

[44] V. S. Tiberkevich, A. N. Slavin, and J.-V. Kim, Phys. Rev. B **78**, 092401 (2008).

[45] B. Georges, J. Grollier, V. Cros, A. Fert, A. Fukushima, H. Kubota, K. Yakushijin, S. Yuasa, and K. Ando, Phys. Rev. B **80**, 060404 (2009).

[46] L. Bianchini, S. Cornelissen, J. Kim, T. Devolder, W. v. Roy, L. Lagae, and C. Chappert, Appl. Phys. Lett. **97**, 032502 (2010).

[47] D. Gusakova, M. Quinsat, J. F. Sierra, U. Ebels, B. Dieny, L. D. Buda-Prejbeanu, M. Cyrille, V. Tiberkevich, and A. N. Slavin, Appl. Phys. Lett. **99**, 052501 (2011).

[48] K. Mizushima, T. Nagasawa, K. Kudo, Y. Saito, and R. Sato, Appl. Phys. Lett. **94**, 152501 (2009).

[49] H. Arai, H. Tsukahara, and H. Imamura, Appl. Phys. Lett. **101**, 092405 (2012).

[50] K. Matsushita, J. Sato, H. Imamura, and M. Sasaki, J. Phys.: Conf. Ser. **200**, 042016 (2010).

[51] T. N. Anh Nguyen, N. Benatmane, V. Fallahi, Y. Fang, S. M. Mohseni, R. K. Dumas, and J. Åkerman, J. Magn. Magn. Mater. **324**, 3929 (2012).